Dyes and Pigments 171 (2019) 107698

Contents lists available at ScienceDirect

Dyes and Pigments

journal homepage: www.elsevier.com/locate/dyepig

Near-infrared squaraine fluorescent probe for imaging adenosine 5′-triphosphate in live cells

Guimei Wang[a,b], Xiaoxue Jiang[a,b], Nanyan Fu[a,b,*]

[a] MOE Key Laboratory for Analytical Science of Food Safety and Biology & Fujian Provincial Key Laboratory of Analysis and Detection Technology for Food Safety, State Key Laboratory of Photocatalysis on Energy and Environment, College of Chemistry, Fuzhou University, Fuzhou, 350116, PR China

[b] Key Laboratory of Bioorganic Phosphorus Chemistry & Chemical Biology (Ministry of Education), Tsinghua University, Beijing, 100084, PR China

ARTICLE INFO

Keywords:
Phenylboronic acid functionalized squaraine
Cetyltrimethyl ammonium bromide (CTAB)
Adenosine 5′-triphosphate (ATP) detection
Supramolecular assembly
NIR fluorescent probe
Bioimaging

ABSTRACT

Adenosine 5′-triphosphate (ATP), as a "molecular currency" for intracellular energy transfer, not only participates in various physiological activities, but also involves in various pathological processes of living cells. Therefore, the establishment of a simple, rapid, sensitive and accurate ATP analysis method is of great significance for the study of its physiological functions. In this work, we rationally design a near-infrared phenylboronic acid group-functionalized dicyanovinyl squaraine (**SQ-PBA3**), with which a supramolecular assembly was constructed for fluorescent imaging of ATP. In PBS buffer, **SQ-PBA3** changes self-assembly when adding cetyltrimethyl ammonium bromide (CTAB) deriving fluorescence response of **SQ-PBA3** to ATP with the maximum emission at 700 nm, due to the specificity of phenylboronic acid to diols and the multiple electrostatic interactions between **SQ-PBA3**, ATP and CTAB molecules. Meanwhile, the probe was successfully applied to monitor intracellular ATP level in MCF-7 cells with high sensitivity and selectivity.

1. Introduction

Adenosine 5′-triphosphate (ATP) is not only a universal energy currency in various cellular activities, but also a signal of many biological processes involved in cell division [1], ion channel [2], DNA synthesis [3], etc. A recent study showed that at micromolar concentrations, ATP can act as a source of energy that drives metabolism in the body, while reaching millimolar concentrations, it in turn serves as a hydrotrope to help solubilize hydrophobic proteins in the cytoplasm [4]. On the other hand, extracellular ATP can function as mediators in tumor metastasis, including cellular proliferation, invasion and death [5]. Therefore, the establishment of a detection method that can be used to monitor changes in ATP level in real time is of great significance for the study of its physiological functions.

Till now, many ATP detection methods have been developed including electrophoresis [6], chemiluminescence [7], bioluminescence [8], and electrochemical analysis [9]. These methods face different challenges in the detection of intracellular ATP, such as the use of off-line methods to obtain cell extracts for analysis by disrupting cells, which will increase the measurement cost, and cannot realize real-time and in-situ detection [10–13]. Compared to these methods, however, fluorescence imaging offers many advantages like simple operation, cost-effectiveness, high sensitivity to analytes, and good selectivity. On top of it all, it can achieve in-situ visible imaging of ATP, which has attracted more and more interest [14–19].

NIR absorbing and emitting fluorescent probes have minimal light damage to organisms, better deep tissue penetration and can effectively reduce background fluorescence from living systems. Squaraine dyes have a non-classical resonance system with a unique zwitterionic structure. The distinctive push-pull electronic structure of the donor-acceptor-donor (D-A-D) results in their strong absorption in the region from red (620–670 nm) to near-infrared. Additionally, squaraine dyes are prone to form diverse aggregates under certain conditions, and these aggregates exhibit distinctly different optical properties from monomers [20–22]. The diversity of dye aggregate forms makes it possible to develop functional fluorescent probes for different target by regulating of the aggregates [23–26].

Boronic acid derivatives can rapidly and reversibly interact with 1,2- or 1,3-diols, which have been widely applied in the recognition of 1,2- or 1,3-diols structure [15,27–30]. In this work, we report a series of dicyanovinyl squaraines (**SQ-PBA1-3**) with boronic acid group in different positions of phenyl ring, whose ability in fluorescent imaging of

* Corresponding author. MOE Key Laboratory for Analytical Science of Food Safety and Biology & Fujian Provincial Key Laboratory of Analysis and Detection Technology for Food Safety, State Key Laboratory of Photocatalysis on Energy and Environment, College of Chemistry, Fuzhou University, Fuzhou, 350116, PR China.

E-mail address: nanyan_fu@fzu.edu.cn (N. Fu).

https://doi.org/10.1016/j.dyepig.2019.107698
Received 25 May 2019; Received in revised form 30 June 2019; Accepted 2 July 2019
Available online 03 July 2019
0143-7208/

ATP in the NIR region have been studied. The phenylboronic acid group is designed as a recognition unit, and an electron withdrawing cyano (–CN) group was introduced in central four-membered ring of squaric acid to improve its photostability. To improve the responsibility of **SQ-PBA1-3** to ATP, supramolecular assemblies were constructed with them and cetyltrimethyl ammonium bromide (CTAB). We speculated that the fluorescence of **SQ-PBA1**-**3** would be quenched due to the aggregation caused quenching (ACQ) effect. Then in the presence of ATP, it will go through a process of disaggregation and reassembly owing to the co-operation of the specificity of phenylboronic acid to diols and the multiple electrostatic interactions between **SQ-PBA1-3**, ATP and CTAB molecules, along with the fluorescence "turn-on", by which time fluorescence imaging of intracellular ATP can be achieved, as well as real-time monitoring of changes in intracellular ATP level.

2. Experimental

2.1. Materials and instruments

Adenosine-5′-triphosphate disodium salt hydrate (ATP), adenosine-5′-diphosphate sodium salt (ADP), adenosine-5′-monophosphate monohydrate (AMP), cytidine-5′-diphosphate disodium salt (CDP), cytidine-5′-triphosphate disodium salt (CTP), uridine-5′-monophosphate disodium salt (UMP), uridine-5′-diphosphate sodium salt (UDP), uridine-5′-triphosphate trisodium salt (UTP), guanosine-5′-monophosphate disodium salt hydrate (GMP), guanosine-5′-diphosphate disodium salt (GDP), and guanosine-5′-triphosphate trisodium salt (GTP) were purchased from Aladdin Reagent Co., Ltd. (Shanghai, China). Other reagents not mentioned above are at least analytically pure, purchased from Sinopharm Chemical Reagent Co., Ltd. (Shanghai, China), and used without further purification; the organic solvents were dried according to standard procedures.

^{1}H NMR (400 MHz) and ^{13}C NMR (100 MHz) spectra were measured on a Bruker AV-400 spectrometer (TMS as internal standard). Absorption spectra were recorded on a PerkinElmer Lambda 750 UV–vis spectrophotometer. Fluorescent emission spectra were acquired using a Cary Eclipse fluorescence spectrophotometer.

2.2. Synthesis

2.2.1. Synthesis of *2*

Dicyanovinyl substituted squaric acid derivative **2** was synthesized according to the reported procedure [31].

2.2.2. Synthesis of *4*

2,3,3-Trimethyl-3*H*-indole (**3**) (120 mg, 0.75 mmol) was dissolved in 4 mL of acetonitrile in a 25 mL round bottom flask, then bromomethyl phenylboronic acid (150 mg, 0.70 mmol) in 4 mL of acetonitrile was injected and refluxed overnight at 80 °C. The solution was dark red and the crude product was purified by column chromatography eluting with dichloromethane: methanol (20:1, v/v) and a khaki solid was obtained.

4a: 170 mg, yield 65%. ^{1}H NMR (400 MHz, DMSO-d_6) δ 7.88 (d, J = 7.2 Hz, 1H), 7.80 (t, J = 4.3 Hz, 1H), 7.58 (d, J = 10.2 Hz, 2H), 7.51 (d, J = 7.6 Hz, 1H), 7.37 (t, J = 4.6 Hz, 2H), 6.93 (t, J = 4.9 Hz, 1H), 6.03 (s, 2H), 2.89 (s, 3H), 1.63 (s, 6H); ^{13}C NMR (100 MHz, DMSO-d_6): δ 198.72, 142.43, 141.91, 136.43, 135.81, 130.89, 129.89, 129.40, 128.00, 125.89, 124.06, 116.32, 54.91, 51.74, 22.60, 15.01; HRMS (ESI) *m/z*: Calcd for $C_{18}H_{21}NBO_2$ ([M]$^+$): 294.1665; found: 294.1656.

4b: 153 mg, yield 58%. ^{1}H NMR (400 MHz, DMSO-d_6) δ 7.88 (d, J = 6.4 Hz, 1H), 7.80 (d, J = 6.9 Hz, 1H), 7.67–7.57 (m, 3H), 7.46 (d, J = 6.7 Hz, 1H), 7.25 (d, J = 6.7 Hz, 1H), 5.84 (s, 2H), 2.99 (s, 3H), 1.62 (s, 6H); ^{13}C NMR (100 MHz, DMSO-d_6): δ 172.44, 161.24, 146.14, 137.36, 136.75, 134.84, 133.12, 128.51, 127.99, 124.08, 122.37, 118.92, 116.40, 105.95, 54.95, 51.33, 21.52, 15.01; HRMS (ESI) *m/z*: Calcd for $C_{18}H_{21}NBO_2$ ([M]$^+$): 294.1665; found: 294.1657.

4c: 140 mg, yield 53%. ^{1}H NMR (400 MHz, DMSO-d_6) δ 7.87 (d, J = 7.0 Hz, 1H), 7.81 (d, J = 7.8 Hz, 2H), 7.78 (d, J = 7.7 Hz, 1H), 7.60 (t, J = 7.2 Hz, 1H), 7.56 (d, J = 7.2 Hz, 1H), 7.37 (d, J = 7.6 Hz, 2H), 5.82 (s, 2H), 2.98 (s, 3H), 1.60 (s, 6H); ^{13}C NMR (100 MHz, DMSO-d_6): δ 198.85, 142.43, 141.91, 136.45, 135.81, 130.89, 129.89, 129.40, 128.00, 125.89, 124.06, 116.32, 54.91, 51.74, 22.60, 15.01; HRMS (ESI) *m/z*: Calcd for $C_{18}H_{21}NBO_2$ ([M]$^+$): 294.1665; found: 294.1657.

2.2.3. Synthesis of *SQ-PBA1-3*

Phenylboronic acid substituted indole **4** (99 mg, 0.265 mmol) and dicyanovinyl substituted squaric acid derivative **2** (38 mg, 0.132 mmol) were dissolved in 20 mL of *n*-butanol and toluene (1:1, v/v) in a 50 mL two-necked flask equipped with a Dean-Stark trap and then the solution was refluxed under nitrogen with stirring for 5 h. The reaction was monitored by thin layer chromatography (TLC) until the completion of the reaction. After that, the solution was cooled to room temperature, washed with water, and dried the organic layer with anhydrous sodium sulfate. After removing the solvent, the residue was purified by column chromatography eluting with dichloromethane: methanol (15:1, v/v) to afford a dark green solid.

SQ-PBA1: 53 mg, yield 56%. ^{1}H NMR (400 MHz, DMSO-d_6): δ 7.75 (d, J = 7.2 Hz, 2H), 7.62 (d, J = 7.3 Hz, 2H), 7.33–7.21 (m, 8H), 7.15 (d, J = 6.9 Hz, 2H), 6.73 (d, J = 7.2Hz, 2H), 6.35 (s, 2H), 5.57 (s, 4H), 1.82 (s, 12H); ^{13}C NMR (100 MHz, DMSO-d_6): δ 172.88, 172.53, 166.65, 165.48, 142.38, 142.27, 133.98, 132.49, 128.70, 128.40, 125.42, 122.85, 118.54, 111.92, 89.06, 79.04, 66.75, 49.81, 47.37, 33.46, 31.99, 31.62, 29.95, 29.47, 26.54, 20.95; HRMS (ESI) *m/z*: Calcd for $C_{43}H_{39}B_2N_4O_5$ ([M + H]$^+$): 713.3107; found: 713.3104.

SQ-PBA2: 33 mg, yield 35%. ^{1}H NMR (400 MHz, DMSO-d_6): δ 7.72–7.63 (m, 8H), 7.37–7.32 (m, 8H), 6.37 (s, 2H), 5.34 (s, 4H), 1.76 (s, 12H); ^{13}C NMR (100 MHz, DMSO-d_6): δ 172.88, 172.53, 166.65, 165.48, 142.38, 142.27, 133.98, 132.49, 128.70, 128.42, 125.42, 122.85, 118.54, 111.91, 89.16, 78.98, 66.79, 49.81, 47.38, 33.42, 32.02, 29.92, 26.54, 20.95; HRMS (ESI) *m/z*: Calcd for $C_{43}H_{39}B_2N_4O_5$ ([M + H]$^+$): 713.3107; found: 713.3101.

SQ-PBA3: 31 mg, yield 33%. ^{1}H NMR (400 MHz, DMSO-d_6): δ 7.74 (d, J = 7.6 Hz, 4H), 7.62 (d, J = 7.2 Hz, 2H), 7.44–7.37 (m, 4H), 7.28 (d, J = 7.3 Hz, 2H), 7.22 (d, J = 7.0 Hz, 4H), 6.34 (s, 2H), 5.33 (s, 4H), 1.74 (s, 12H); ^{13}C NMR (100 MHz, DMSO-d_6): δ 172.76, 172.40, 172.39, 165.45, 142.44, 142.25, 137.00, 135.10, 128.76, 126.06, 125.47, 122.90, 118.56, 111.86, 89.20, 49.78, 47.30, 33.42, 32.07, 29.47, 26.52, 20.95; HRMS (ESI) *m/z*: Calcd for $C_{43}H_{39}B_2N_4O_5$ ([M + H]$^+$): 713.3107; found: 713.3140.

2.3. General procedure for spectral measurement

Stock solutions of **SQ-PBA1**-**3** (10 mM) were prepared by dissolving them in DMSO. A stock solution of ATP (10 mM) was prepared in twice distilled water. Solutions of AMP, ADP, CDP, CTP, GMP, GDP, GTP, UMP, UDP, UTP were prepared in twice distilled water (50 mM), respectively. 0.8 μL of **SQ-PBA1**-**3** stock solutions were added to 2 mL of PBS buffer solutions (10 mM, pH 7.4) in quartz cuvettes of 1 cm path length to acquire 4.0 μM dye solutions, and different volumes of the ATP solutions were added.

2.4. Dynamic light scattering measurement (DLS)

Solutions of **SQ-PBA3**, CTAB and ATP were filtered through a filter membrane with a pore size of 0.25 μm, and then transferred to clean cuvettes for testing.

2.5. Field emission scanning electron microscope (FESEM)

Solutions of **SQ-PBA3** alone in PBS solution, in the presence of surfactant CTAB (0.25 mM) and subsequently addition of ATP were

prepared respectively. After standing at room temperature for 20 min, a drop of the solution was added on the cleaned single crystal silicon wafer, evaporated at room temperature, and tested after spraying gold.

2.6. Cell incubation and fluorescence microscopy imaging

The MCF-7 cells were cultivated in a 35 mm confocal culture dish in an atmosphere of 5% CO_2 at 37°C in DEME culture medium containing 10% fetal bovine serum (FBS), 1.0% penicillins and treptomycin. After incubation for 24 h, the MCF-7 cells were further treated with 4.0 μM **SQ-PBA3** at 37 °C for 1.5 h. Following the removal of the culture medium, the cells were washed with PBS buffer three times and then incubated with 10 nM paclitaxel in DEME culture medium for 24 h. Fluorescence imaging was performed on a Nikon confocal microscope C2/C2si.

3. Results and discussion

3.1. Synthesis and sensing mechanism of supramolecular assembly

The chemical structure and synthetic procedure of **SQ-PBA1-3** are summarized in Scheme 1. Substitution reaction between bromomethyl phenylboronic acid and 2,3,3-trimethyl-3*H*-indole (**3**) gave compound **4**. **SQ-PBA1-3** were prepared by condensation reaction between dicyanovinyl substituted squaric acid derivative **2** and phenylboronic acid substituted indole **4**, and characterized by ^{1}H NMR, ^{13}C NMR, and high-resolution mass spectrometry (Figs. S1–S18, Supplementary Data).

As shown in Scheme 2, the proposed sensing supramolecular assembly was composed of ATP probe and CTAB. When **SQ-PBA3** alone is dissolved in PBS solution, the molecules are self-aggregated due to hydrophobic interaction and π-π interaction, leading to the fluorescence quenching. With further addition of CTAB, the electrostatic interaction between **SQ-PBA3** and CTAB would change the aggregates of the probe, contributing to the sensing of ATP. In order to obtain a low background signal, the concentration of CTAB should be optimized. In the presence of ATP, the molecules are reassembled to form a short and small rod-like structure owing to the electrostatic interaction between the **SQ-PBA3**, ATP and CTAB molecules, accompanied by the fluorescence "turn-on" of **SQ-PBA3**.

3.2. Construction of supramolecular assembly

In order to improve the response of compounds under physiological conditions, we first studied the effect of different surfactants on the ATP response ability of **SQ-PBA3**. The cationic surfactant CTAB and the nonionic surfactant Tween 80 (TW80) were added into PBS buffer (pH = 7.4, 10 mM), respectively, then the same amount of ATP was added for UV–Vis spectral analysis. It was found from Fig. S19 (Supplementary Data), that the absorption of the monomer around 680 nm was significantly enhanced with a bathochromic shift only in the presence of CTAB, indicating that CTAB was helpful to improve the response of **SQ-PBA3** to ATP. This may be attributed to the electrostatic interaction between **SQ-PBA3** and CTAB, which can modulate the aggregation state of dye.

The concentration of CTAB was then optimized. Absorbance changes of **SQ-PBA3** solutions before and after the addition of ATP were measured with different concentrations of CTAB. The results are shown in Fig. 1. When the concentration of CTAB is 0.25 mM, the absorbance change of the solution is the largest, indicating the formation of the supramolecular assembly. Thus it is determined that 0.25 mM is the best test concentration.

3.3. Spectral response of supramolecular assemblies to AMP, ADP and ATP

Firstly, we studied the fluorescence response of supramolecular assemblies to AMP, ADP and ATP in PBS buffer solution (pH = 7.4, 10 mM, 0.25 mM CTAB). As shown in Fig. 2, supramolecular assembly containing **SQ-PBA2** displayed no response to AMP, ADP and ATP,

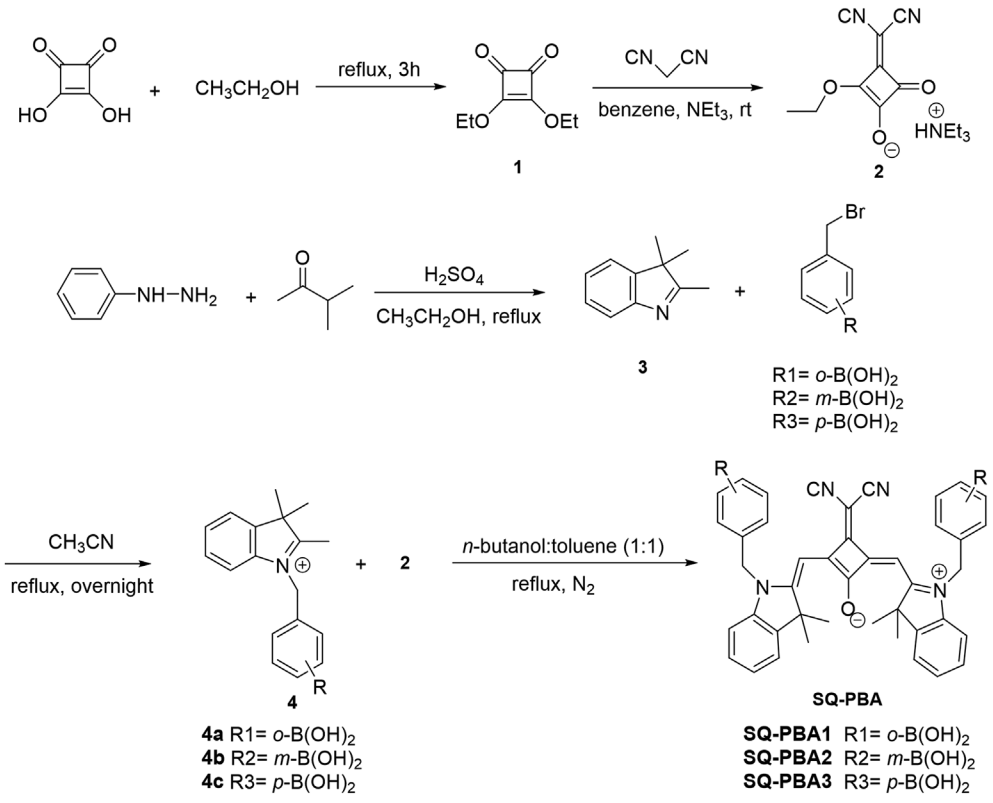

Scheme 1. Synthesis of **SQ-PBA1-3**.

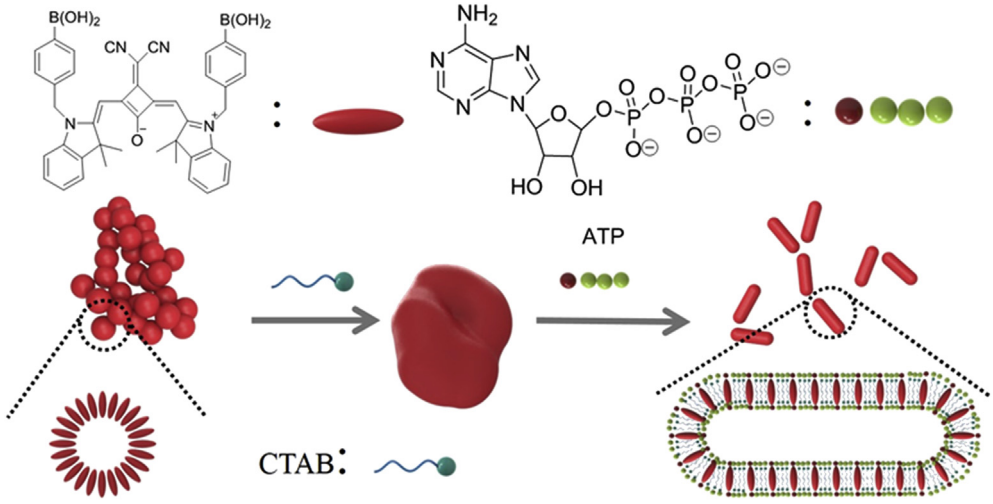

Scheme 2. Schematic illustration of self-assembly of squaraine dye **SQ-PBA3** in aqueous solution and detection of ATP.

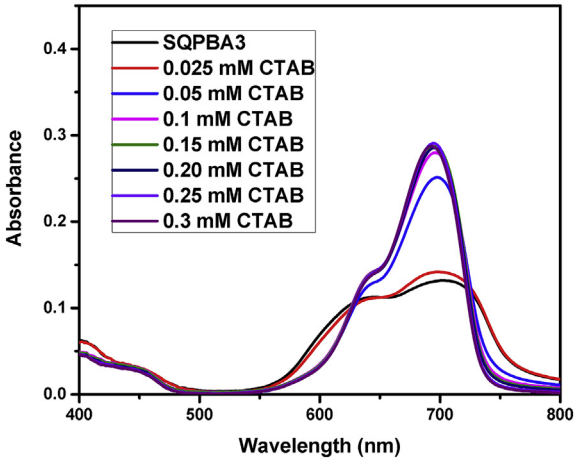

Fig. 1. Absorption spectra of **SQ-PBA3** (4.0 μM) in PBS solution (pH = 7.4, 10 mM) in the presence of increasing concentration of CTAB from 0 to 0.3 mM.

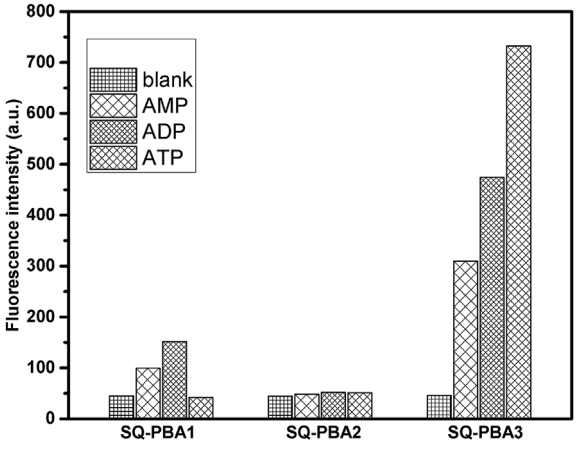

Fig. 2. Fluorescence spectra of **SQ-PBA1-3** responding to ATP. (λex = 670 nm, slit: 5 nm/5 nm, PMT Volts: 650).

while **SQ-PBA1** and **SQ-PBA3** all exhibited different levels of fluorescence response to ATP, and the strongest fluorescence response of **SQ-PBA3** to ATP was observed. This result may be ascribed to the electron effect on the benzene ring. Although the *ortho*-position substitution is responsive to ATP, it is not conducive to the recognition due to the large

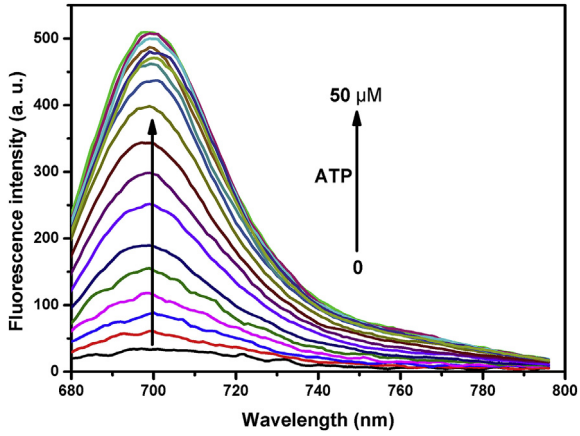

Fig. 3. Fluorescence spectra of **SQ-PBA3** with the increasing addition of ATP in PBS solution (pH = 7.4, 10 mM, 0.25 mM CTAB).

space steric hindrance of the *ortho* position. Thus, **SQ-PBA3** was chosen to evaluate its response towards ATP.

Following, we performed ATP fluorescence titration experiments in PBS solution (pH = 7.4, 10 mM, 0.25 mM CTAB). Fig. 3 shows the fluorescence spectra of **SQ-PBA3** with different amounts of ATP. It can be seen that the fluorescence of **SQ-PBA3** in PBS solution was weakly fluorescent, with the addition of ATP, gradual increase in the fluorescence intensity at 700 nm was found, and then the saturated fluorescence intensity with a 15-fold enhancement was obtained upon the addition of 40 μM ATP. As shown in Fig. S20 (Supplementary Data), a good linear relationship was discovered between the fluorescence intensity of the solution and the ATP concentration from 2 to 22 μM (R^2 = 0.9918, $k = 3.12 \times 10^8$). According to $3\sigma/k$, the calculated detection limit is 28 nM.

The relative amount of ATP and its dephosphorylated products ADP and AMP, control the metabolic activity of the cell. Thus, we performed AMP, ADP and ATP fluorescence titration experiments in PBS solution (pH = 7.4, 10 mM, 0.25 mM CTAB). As can be seen in Fig. 4a, **SQ-PBA3** exhibited different response towards AMP, ADP and ATP, and the addition of ATP lead to the largest increases of fluorescence, which was about 2 times of ADP and 3 times of AMP.

3.4. The specificity of *SQ-PBA3* to ATP

Meanwhile we examined the specificity of **SQ-PBA3** to ATP over some metal ions, amino acids and nucleotides present in biological

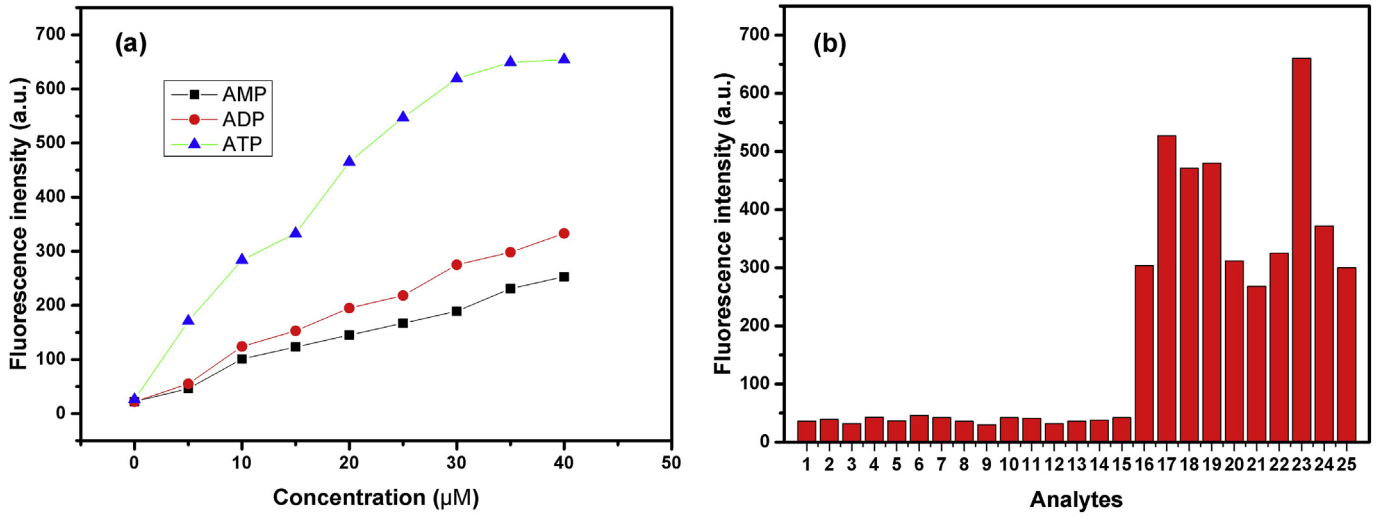

Fig. 4. (a) Fluorescence titration curve of **SQ-PBA3** (4.0 μM) in PBS solution (pH = 7.4, 10 mM, 0.25 mM CTAB) upon the addition of ATP (blue), ADP (red) and AMP (black). (b) The fluorescence response of **SQ-PBA3** (4.0 μM) in the PBS solution (pH = 7.2, 10 mM, 0.25 mM CTAB) in the presence of 5 mM proline (1), histidine (2), cysteine (3), arginine (4), GSH (5), lysine (6), glutamic acid (7), asparaginic acid (8), tyrosine (9), serine (10), Zn^{2+} (11), Na^{+} (12), K^{+} (13), Mg^{2+} (14), Ca^{2+} (15), CDP (16), CTP (17), UTP (18), GTP (19), UMP (20), AMP (21), ADP (22), ATP (23), GDP (24), UDP (25). (λ_{ex} = 670 nm, slit: 5 nm/5 nm, PMT Volts: 650). (For interpretation of the references to colour in this figure legend, the reader is referred to the Web version of this article.)

systems by recording fluorescence spectra of **SQ-PBA3**. Due to the similarity of nucleotide structures, such as UTP, GTP and CTP, these substances all induced increase of fluorescence (Fig. 4b), which may indirectly indicate that the recognition of ATP is mainly due to the specificity of phenylboronic acid to diols. ATP plays a major role in the energy metabolism of the human body. The release and absorption of energy in the body is mainly manifested by the production and consumption of ATP. In addition, UTP, CTP and GTP are also sources of energy in the anabolism of some substances. Thus **SQ-PBA3** can be used to monitor changes in the total intracellular nucleoside triphosphate content caused by drugs or diseases.

3.5. Response mechanism

First, the binding ratio between the **SQ-PBA3** and ATP was studied by Job's Plot experiment. The change of the maximum absorbance of solution increases linearly with the increase of the ATP concentration. Then the inflection point occurs when [ATP]/[ATP] + [**SQ-PBA3**] is 0.67, so the binding ratio of ATP to **SQ-PBA3** is 2:1 (Fig. S21, Supplementary Data).

To further confirm that ATP induced reassembly of **SQ-PBA3** in aqueous solution, we conducted dynamic light scattering experiments (DLS) to study the particle size distribution of aggregates. As shown in Fig. 5, the average hydrated particle size of **SQ-PBA3** in PBS buffer solution is 570 nm. When the CTAB was added to the solution, the particle size decreased to 120 nm, indicating that CTAB has a good solubilizing effect on the dye, which is consistent with the experimental results of the absorbance spectrum. With the subsequent addition of ATP, the particle size of the solution was further decreased to 70 nm. All the results revealed the reassembly of **SQ-PBA3** by the addition of ATP.

The aggregates morphology of **SQ-PBA3** alone in PBS solution, in the presence of surfactant CTAB and subsequently addition of ATP were observed respectively by field emission scanning electron microscopy. When **SQ-PBA3** was alone in PBS solution, it self-aggregated and agglomerated together in the form of small spheres (Fig. 6a). After adding CTAB, the morphology of the aggregates changed greatly (Fig. 6b). With further addition of ATP, the agglomerated aggregates in the solution disappeared, exhibiting a short and small rod-like structure, and the structures spread in a dendritic shape (Fig. 6c).

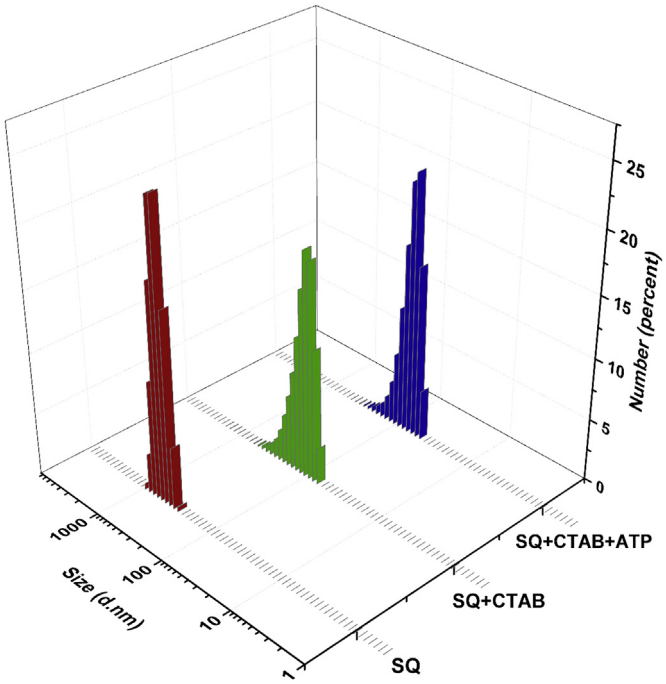

Fig. 5. DLS analysis of **SQ-PBA3** (4.0 μM) alone, in the presence of CTAB, and CTAB + ATP in PBS solution (pH = 7.4, 10 mM).

3.6. Intracellular imaging for endogenous ATP

We then examined the capacity of **SQ-PBA3** to monitor ATP levels in living cells. Paclitaxel was used for fluorescence imaging because it interferes with the normal function of the cytoskeletal component microtubules, stopping cell division in mitosis, until death [32]. It can be seen from Fig. 7 that MCF-7 cells incubated with 4.0 μM **SQ-PBA3** displayed bright red fluorescence and have good dispersion in the cells, indicating that the probe has good cell permeability. The cells continued to be incubated with paclitaxel, as expected, showed significantly weakened fluorescence, suggesting that the decreased ATP level in the cells and the abilities of **SQ-PBA3** to sense the changes of intracellular ATP level.

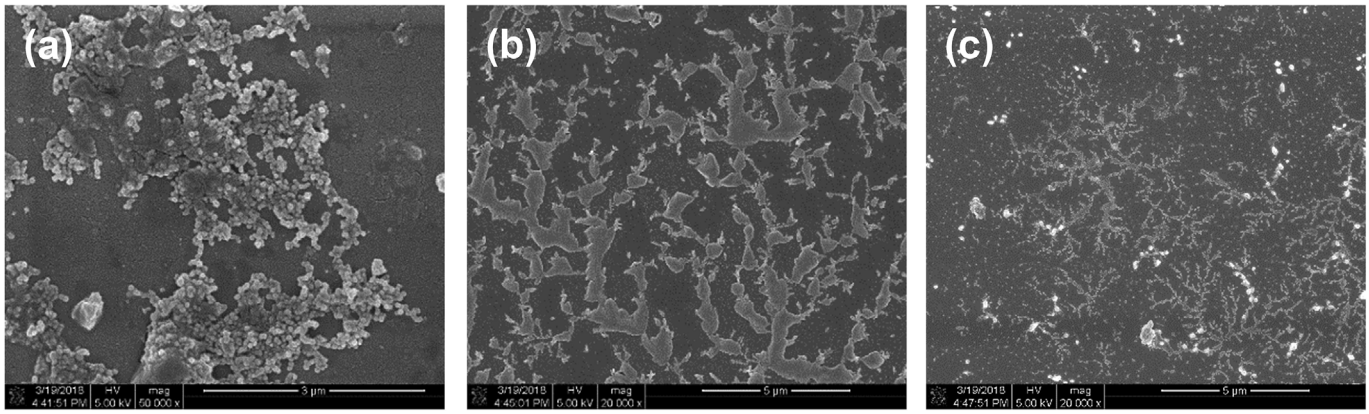

Fig. 6. FESEM images of **SQ-PBA3** (4.0 μM) in PBS solution (pH = 7.4, 10 mM) (a), with 0.25 mM CTAB (b), with 0.25 mM CTAB and 40 μM ATP (c).

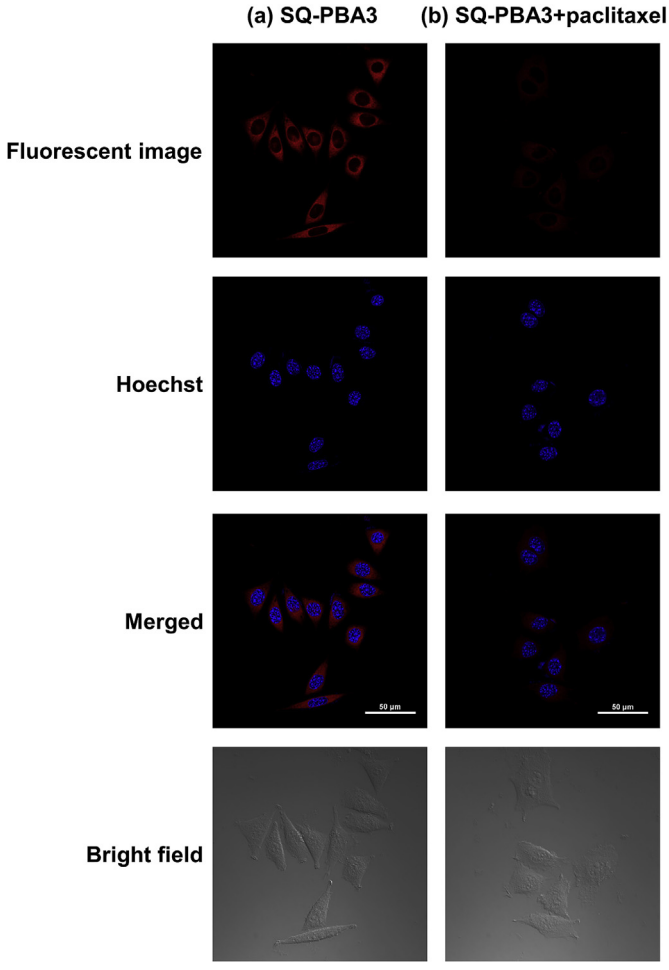

Fig. 7. Fluorescent images of MCF-7 cells. (a) MCF-7 cells incubated with **SQ-PBA3** for 2 h, (b) pretreated with **SQ-PBA3** for 2 h and further incubated with paclitaxel (10 nM) for 24 h.

4. Conclusion

In conclusion, based on multisite combining and "aggregation-re-assembly" strategies, we have developed a near-infrared squaraine (**SQ-PBA3**) attached with two phenylboronic acid groups for selectively and sensitively detection of ATP in living cells. The dye can effectively monitor changes in intracellular ATP level. We expect that our work should provide new attempts for the design of near-infrared squaraine based fluorescent probes for biosensing detection with higher sensitivity and better selectivity.

Acknowledgements

This work was financially supported by the Program for Chang Jiang Scholars and Innovative Research Team in University of Ministry of Education of China (IRT15R11), the Fujian Provincial Natural Science Foundation, P.R. China (No. 2017J01577, 2019J01208), the Open Project Program of the State Key Laboratory of Photocatalysis on Energy and Environment, Fuzhou University (No. SKLPEE-KF201724, SKLPEEKF201727), and the Open Project Program of Key Laboratory of Bioorganic Phosphorus Chemistry & Chemical Biology (Ministry of Education), Tsinghua University.

Appendix A. Supplementary data

Supplementary data to this article can be found online at https://doi.org/10.1016/j.dyepig.2019.107698.

References

[1] Shen X, Mizuguchi G, Hamiche A, Wu C. A chromatin remodelling complex involved in transcription and DNA processing. Nature 2000;406:541–4.
[2] Ashcroft FM, Gribble FM. ATP-sensitive K^+ channels and insulin secretion: their role in health and disease. Diabetologia 1999;42:903–19.
[3] Dennis PB, Jaeschke A, Saitoh M, Fowler B, Kozma SC, Thomas G. Mammalian TOR: a homeostatic ATP sensor. Science 2001;294:1102–5.
[4] Patel A, Malinovska L, Saha S, Wang J, Alberti S, Krishnan Y, Hyman AA. Biochemistry: ATP as a biological hydrotrope. Science 2017;356:753–6.
[5] Liu Y, Geng YH, Yang H, Yang H, Zhou YT, Zhang HQ, Tian XX, Fang WG. Extracellular ATP drives breast cancer cell migration and metastasis via S100A4 production by cancer cells and fibroblasts. Cancer Lett 2018;430:1–10.
[6] Yangyuoru PM, Dhakal S, Yu Z, Koirala D, Mwongela SM, Mao H. Single-molecule measurements of the binding between small molecules and DNA aptamers. Anal Chem 2012;84:5298–303.
[7] Zhang S, Yan Y, Bi S. Design of molecular beacon as signaling probes for ATP detection in cancer cells based on chemiluminescence resonance energy transfer. Anal Chem 2009;81:8695–701.
[8] Liu BF, Ozaki M, Hisamoto H, Luo Q, Utsumi Y, Hattori T, Terabe S. Microfluidic chip toward cellular ATP and ATP-conjugated metabolic analysis with bioluminescence detection. Anal Chem 2005;77:573–8.
[9] Goyal RN, Oyama M, Singh SP. Simultaneous determination of adenosine and adenosine-5'-triphosphate at nanogold modified indium tin oxide electrode by osteryoung square-wave voltammetry. Electroanalysis 2007;19:575–81.
[10] Manfredi G, Yang L, Gajewski CD, Mattiazzi M. Measurements of ATP in mammalian cells. Methods 2002;26:317–26.
[11] Li M, Zhang J, Suri S, Sooter LJ, Ma D, Wu N. Detection of adenosine triphosphate with an aptamer biosensor based on surface-enhanced Raman scattering. Anal Chem 2012;84:2837–42.
[12] Gout E, Rebeille F, Douce R, Bligny R. Interplay of Mg^{2+}, ADP, and ATP in the cytosol and mitochondria: unravelling the role of Mg^{2+} in cell respiration. Proc Natl Acad Sci Unit States Am 2014;111:E4560–7.
[13] Wang G, Su X, Xu Q, Xu G, Lin J, Luo X. Antifouling aptasensor for the detection of adenosine triphosphate in biological media based on mixed self-assembled aptamer and zwitterionic peptide. Biosens Bioelectron 2018;101:129–34.
[14] Xu Z, Singh NJ, Lim J, Pan J, Ha NK, Park S, Kim KS, Yoon J. Unique sandwich

stacking of pyrene-adenine-pyrene for selective and ratiometric fluorescent sensing of ATP at physiological pH. J Am Chem Soc 2009;131:15528–33.
[15] Wang L, Yuan L, Zeng X, Peng J, Ni Y, Er JC, Xu W, Agrawalla BK, Su D, Kim B, Chang YT. A multisite-binding switchable fluorescent probe for monitoring mitochondrial ATP level fluctuation in live cells. Angew Chem Int Ed 2016;55:1773–6.
[16] Tan KY, Li CY, Li YF, Fei J, Yang B, Fu YJ, Li F. Real-time monitoring ATP in mitochondrion of living cells: a specific fluorescent probe for ATP by dual recognition sites. Anal Chem 2017;89:1749–56.
[17] Zhang M, Ma WJ, He CT, Jiang L, Lu TB. Highly selective recognition and fluorescence imaging of adenosine polyphosphates in aqueous solution. Inorg Chem 2013;52:4873–9.
[18] Liu Y, Lee D, Wu D, Swamy KMK, Yoon J. A new kind of rhodamine-based fluorescence turn-on probe for monitoring ATP in mitochondria. Sensor Actuator B Chem 2018;265:429–34.
[19] Liu JH, Li RS, Yuan B, Wang J, Li YF, Huang CZ. Mitochondria-targeting single-layered graphene quantum dots with dual recognition sites for ATP imaging in living cells. Nanoscale 2018;10:17402–8.
[20] Chen H, Law KY, Perlstein J, Whitten DG. Amphiphilic squaraine dye aggregates: evidence for a cyclic chiral structure as a general supramolecular structure for aggregates of dyes and aromatic molecules. J Am Chem Soc 1995;117:7257–8.
[21] De Miguel G, Ziółek M, Zitnan M, Organero JA, Pandey SS, Hayase S, Douhal A. Photophysics of H- and J-aggregates of indole-based squaraines in solid state. J Phys Chem C 2012;116:9379–89.
[22] Xu Y, Li Z, Malkovskiy A, Sun S, Pang Y. Aggregation control of squaraines and their use as near-infrared fluorescent sensors for protein. J Phys Chem B 2010;114:8574–80.
[23] Chen C, Wang R, Guo L, Fu N, Dong H, Yuan Y. A squaraine-based colorimetric and "turn on" fluorescent sensor for selective detection of Hg^{2+} in an aqueous medium. Org Lett 2011;13:1162–5.
[24] Anees P, Sreejith S, Ajayaghosh A. Self-assembled near-infrared dye nanoparticles as a selective protein sensor by activation of a dormant fluorophore. J Am Chem Soc 2014;136:13233–9.
[25] Wang G, Xu W, Guo Y, Fu N. Near-infrared squaraine dye as a selective protein sensor based on self-assembly. Sensor Actuator B Chem 2017;245:932–7.
[26] Sun P, Wu Q, Sun X, Miao H, Deng W, Zhang W, Fan Q, Huang W. J-Aggregate squaraine nanoparticles with bright NIR-II fluorescence for imaging guided photothermal therapy. Chem Commun 2018;54:13395–8.
[27] Ma R, Yang H, Li Z, Liu G, Sun X, Liu X, An Y, Shi L. Phenylboronic acid-based complex micelles with enhanced glucose-responsiveness at physiological pH by complexation with glycopolymer. Biomacromolecules 2012;13:3409–17.
[28] Yang H, Sun X, Liu G, Ma R, Li Z, An Y, Shi L. Glucose-responsive complex micelles for self-regulated release of insulin under physiological conditions. Soft Matter 2013;9:8589–99.
[29] Sun X, Xu Q, Kim G, Flower SE, Lowe JP, Yoon J, Fossey JS, Qian X, Bull SD, James TD. A water-soluble boronate-based fluorescent probe for the selective detection of peroxynitrite and imaging in living cells. Chem Sci 2014;5:3368–73.
[30] Zhang P, Zhu MS, Luo H, Zhang Q, Guo LE, Li Z, Jiang YB. Aggregation-switching strategy for promoting fluorescent sensing of biologically relevant species: a simple near-infrared cyanine dye highly sensitive and selective for ATP. Anal Chem 2017;89:6210–5.
[31] Mayerhöffer U, Fimmel B, Würthner F. Bright near-infrared fluorophores based on squaraines by unexpected halogen effects. Angew Chem Int Ed 2012;51:164–7.
[32] Alushin GM, Lander GC, Kellogg EH, Zhang R, Baker D, Nogales E. High-Resolution microtubule structures reveal the structural transitions in α β-tubulin upon GTP hydrolysis. Cell 2014;157:1117–29.